Aust. J. Phys., 1984, **37**, 137–56

The LT-4 Tokamak. I Description of the Apparatus and Its Operation

M. G. Bell,[A] *A. D. Cheetham, S. M. Hamberger, G. R. Hogg*,[B] *M. J. Hollis, J. A. How, H. Kuwahara, A. H. Morton, L. E. Sharp, L. B. Whitbourn*[C] *and C. F. Vance*

Plasma Research Laboratory, Research School of Physical Sciences, Australian National University, G.P.O. Box 4, Canberra, A.C.T. 2601.
[A] Present address: Princeton Plasma Physics Laboratory, P.O. Box 451, Princeton, NJ 08544, U.S.A.
[B] Present address: Australian Atomic Energy Commission Research Establishment, Lucas Heights Research Laboratories, Private Mailbag, Sutherland, N.S.W. 2232.
[C] Present address: Division of Applied Physics, CSIRO, P.O. Box 218, Lindfield, N.S.W. 2070.

Abstract

The LT-4 is a relatively small (major radius 0·5 m, minor radius ~0·1 m) experimental tokamak using a homopolar generator as its main power source to produce a toroidal field of 3 T. A fast current-forcing feedback control system maintains the plasma position constant to ~1 mm. Fairly standard diagnostics are supported by a data acquisition system which handles 200 kbytes of data through 70 CAMAC controlled ADCs per discharge. Illustrative examples of data obtained during typical operation show magnetohydrodynamic (MHD) activity (magnetic pick-up coils and soft X-ray detectors) as well as relaxation oscillations within the plasma.

1. Introduction

The LT-4 tokamak is an experimental apparatus for studying the properties and behaviour of a toroidal column of hot, fully ionized plasma confined by strong magnetic fields. It is a representative example of many tokamaks currently operating around the world, all based on essentially similar principles, being used for research directed towards the achievement of controlled thermonuclear fusion power. While LT-4 is small compared with a number of others, especially those recently brought into operation such as JET (Rebut 1984) and TFTR (Young 1984) which are expected to achieve reactor-like or even fusion ignition conditions, its performance and its own special features enable it to be used to investigate many important aspects of plasma behaviour which are not yet fully understood, although directly relevant to the conditions of a magnetically controlled fusion reactor.

For the benefit of readers not already familiar with the field, a brief outline of the principles of the tokamak equilibrium configuration is given in the Appendix. For a more detailed discussion see the reviews by Artsimovich (1972), Furth (1975), Bickerton (1977) and Sheffield (1981).

In the Australian context, LT-4 is a successor to earlier tokamaks operated at the Australian National University since 1965 (Morton 1981), i.e. for several years before the rapid expansion of interest overseas in such devices (post-1970). It is unique in being the only plasma apparatus to derive the large electrical power

0004-9506/84/020137$02.00

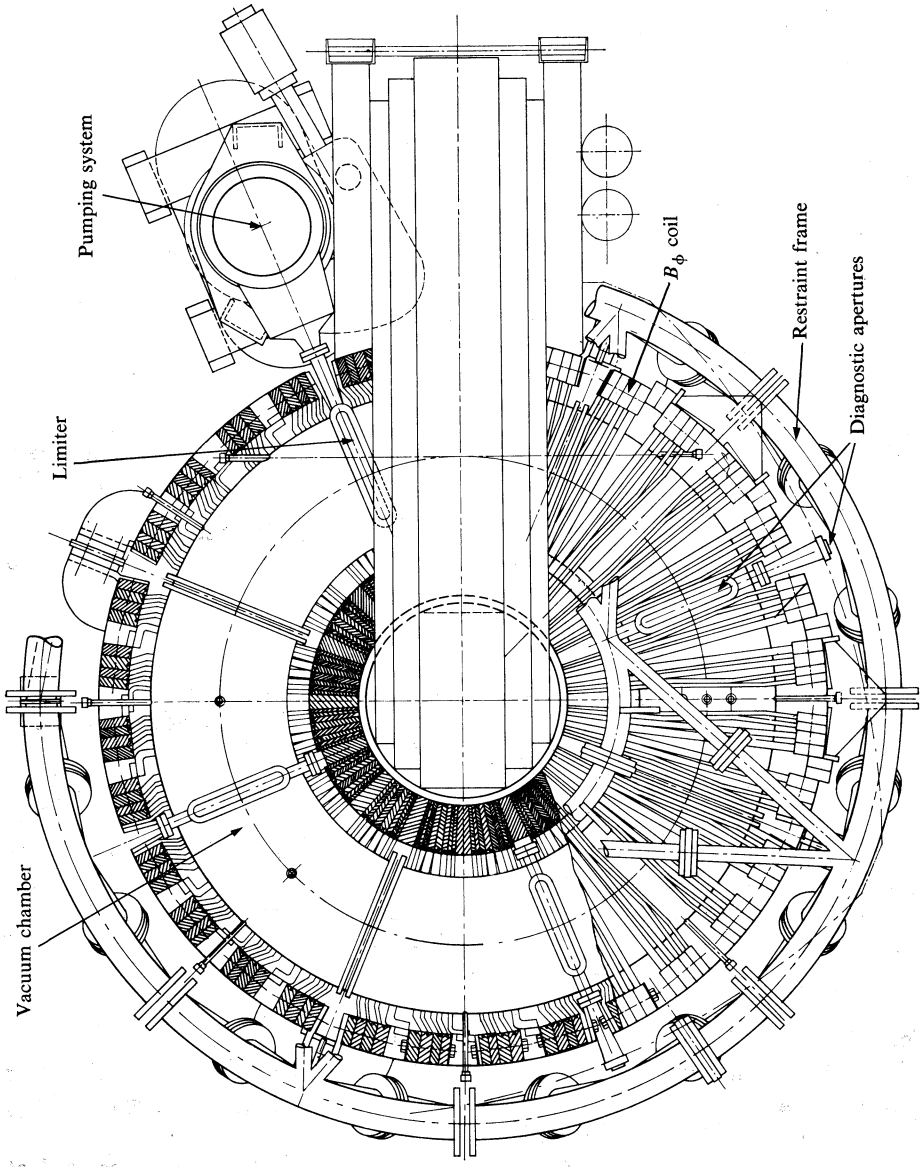

Fig. 1. Plan view of LT-4 showing the iron core, toroidal field coils, restraint frame and vacuum chamber.

required for its toroidal magnet from a homopolar generator (HPG) (Blamey 1978), although several design studies on the use of similar stored energy supplies to power tokamaks have been made in the United States (see e.g. Weldon *et al.* 1978).

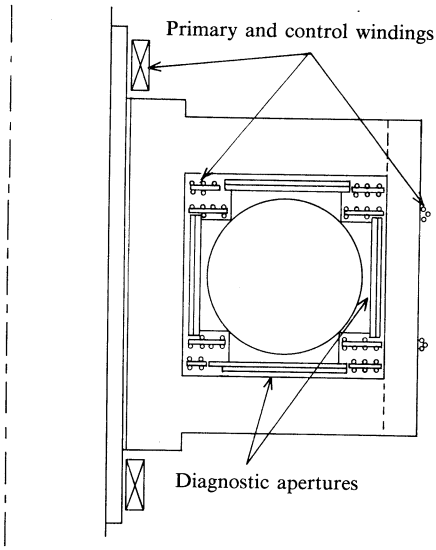

Fig. 2. Section of LT-4 showing the position of the poloidal field windings relative to the vacuum chamber and toroidal field coils.

The organization of the paper is as follows: the apparatus and its associated power supplies are described in Section 2; some of the principal diagnostics and their chief functions are outlined in Section 3; an outline of typical operating conditions is given in Section 4, with some concluding remarks in Section 5. Detailed results on specific topics will be presented in subsequent papers.

Table 1. Main dimensions and operating parameters of the LT-4 tokamak

Parameter	Value
Mean major radius	$R_0 = 0{\cdot}5$ m
Minor radius of vacuum vessel	$b = 0{\cdot}14$ m
Minor plasma radius (normal operation)	$a = 0{\cdot}10$ m
Toroidal field (max.)	$B_0 = 3$ T
Plasma current (max.)	$I_p = 70$ kA
Available flux swing of transformer	0·3 V s
Plasma duration (max.)	160 ms
Interval between pulses	4–5 min
Typical mean plasma density	$\bar{n} = 3\times10^{19}$ m^{-3}
Electron temp.: peak on minor axis	$T_0 = 500$ eV
Typical energy confinement time	$\tau_E \sim 0{\cdot}5$ ms

2. Description of LT-4

The apparatus is shown schematically in Figs 1 and 2 and the main dimensions and operating parameters are listed in Table 1.

(a) Torus and Vacuum System

The vacuum chamber is constructed from 1·5 mm thick Inconel 600 alloy, formed into quadrants which are electrically insulated from each other by 10 mm thick alumina rings and with demountable 0·5 mm diameter gold wire vacuum seals. The use of thin walls of high resistivity material corresponds to short magnetic field penetration times ($\sim 100\ \mu s$). The torus is evacuated by a 400 $L\,s^{-1}$ turbomolecular pump via a high conductance (200 $L\,s^{-1}$) line, while gas (usually palladium-filtered pure hydrogen) is admitted via a combination of fine control mechanical and piezo-electrically operated valves, which can be either pre-programmed or servo-controlled.

Diagnostic and other physical access to the plasma is via four sets of rectangular 200×20 mm viewing apertures plus eighteen 9·5 mm diameter ports (see Fig. 1) providing both radial and tangential viewing; access is also available through the pump line both for diagnostic purposes and for servicing the limiters, which are located at a position close to the pump port.

The vacuum system is oil free, and considerable care is taken with cleanliness. Indium is used wherever gold or copper seals are impracticable (e.g. on optical windows).

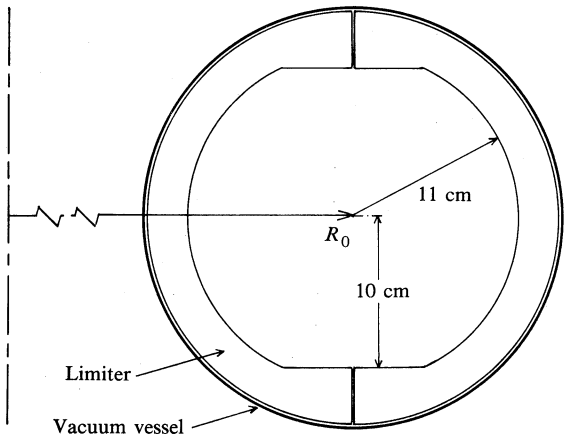

Fig. 3. Diagram of the fixed limiter.

The residual gas content of the system is monitored by a quadrupole mass spectrometer (Quadruvac Type Q200). For satisfactory tokamak operation (i.e. following discharge cleaning q.v.) the base pressure must be $\sim 2 \times 10^{-8}$ Torr (1 Torr = 133 Pa), the residual gas consisting mainly of water vapour. Initial hydrogen filling pressure is typically 0·06 mTorr H_2 followed by programmed gas injection to maintain the desired plasma density. Currently the machine is operated with a stainless steel limiter (Fig. 3) which allows a plasma column of minor radius $a = 10$ cm to be positioned with its centre on the equatorial plane $z = 0$ and up to 1 cm on either side of the geometric centre of the torus, $R_0 = 50$ cm. A second vertical, movable limiter allows the plasma radius to be reduced to less than 10 cm.

(b) Toroidal Magnetic Field

The main (toroidal) field winding consists of 128 rectangular turns of edge-water-cooled solid copper conductors arranged as shown in Fig. 1. The coil is demountable,

each turn consisting of a fabricated lazy U-section completed (on the outside) by bolted-on vertical bars. The coil is arranged in identical quadrants, each quadrant being split into mirror-imaged octants consisting of 16 series turns in groups of eight. At the maximum operating field of 3 T, each octant carries approximately 60 kA.

The spacing, thickness and layout of the conductors has been optimized so as to maintain a high degree of field regularity despite being necessarily non-uniformly spaced because of the diagnostic and pump ports. The field spatial ripple of 1% at $r = 10$ cm falls rapidly at smaller radii (i.e. inside the plasma) and is negligibly small near the centre.

Systematic field errors are kept small by careful mechanical alignment: a typical ratio of residual radial/toroidal fields is less than 10^{-3}, as measured by electron beam orbits. However, for optimal operation (see Section 4) it is found necessary to compensate for the residual transverse error fields, using ancillary windings, to better than $1 : 10^4$. If this is not done, initial gas breakdown is adversely affected, and more runaway electrons are produced.

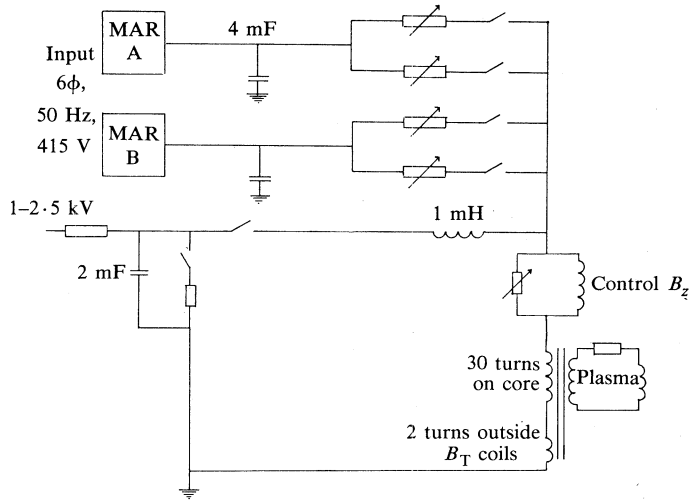

Fig. 4. Circuit diagram of the ohmic heating and vertical field system.

For normal operation the coil octants are connected in parallel to the HPG busbar. The current pulse is initiated by a hydraulically operated fast mechanical switch, and subsequently controlled by a variable electrolytic resistor which also acts as circuit breaker (Hollis 1978). Peak currents are typically 0·45 MA, and the pulse duration is about 1 s. For the duration of the longest tokamak discharges the field can be maintained to $\pm 1\%$.

In the discharge cleaning mode the winding octants are connected in series and energized by a capacitor bank discharge, normally producing fairly low fields ($B < 0{\cdot}2$ T).

The coils are constrained against the strong inward radial forces (during the field rise) by wedges between their inner limbs (which also serve to make the coil set self-supporting) and against outward relaxation (after peak field) by pre-stressed fibre-glass rings. In addition, each group of turns in the assembly is positively located

(with respect to the laboratory) by a rigid stainless-steel restraint frame, which also prevents coil rotation due to the various torques introduced (see Fig. 1).

(*c*) *Ohmic Heating (OH) Circuit*

The plasma current is induced using the transformer arrangement shown schematically in Fig. 4. The transformer core is reverse biassed almost to saturation to allow the maximum possible flux swing of about 0·3 V s. The available primary windings (Fig. 2) are located mainly on the central limb of the core, with others outside the toroidal field coils and in the space between the torus and the field coils, the arrangement being such as to make the primary current provide part of the transverse field B_z required for equilibrium (see the Appendix). The close-coupled transformer arrangement makes the primary and secondary currents approximately proportional before the core starts to saturate, i.e. related to the turns ratio which is usually around 30 : 1.

Primary current is supplied from a passively crowbarred capacitor bank discharge, whose main function is to bring the plasma current up to its maximum value fairly rapidly (<10 ms), and from the mains by two high power six-phase (6ϕ) grid-controlled mercury arc rectifiers (MAR), which can maintain a constant primary current or have it arbitrarily varied on a time scale of ~ 10 ms (determined by the 300 Hz ripple filter). The maximum pulse duration is set by core saturation; for normal operation with clean low resistance plasma exhibiting a low level of magnetohydrodynamic activity (loop voltage 1·5–2 V) it is around 160 ms. The present system is capable of producing plasma currents up to 100 kA: however, if good current control and maximum duration pulses are required, the transformer characteristics restrict the current to about 75 kA. For most experiments the discharge is terminated (by switching off the rectifier) after 100 ms.

For discharge cleaning only four primary turns are used, connected in series with the toroidal field coil, and powered by the capacitor bank alone. The repetition rate in this mode is about one discharge every four seconds.

(*d*) *Control and Correction Fields*

In order to maintain the equilibrium field arrangement (see the Appendix) it is necessary at all times in the discharge sequence to:

(1) Correct for stray magnetic fields due to slight coil misalignment, flux leakage from the transformer, unavoidable dipole fields due to current feeds, the Earth's magnetic field, etc.

(2) Provide the necessary vertical field of magnitude given by equation (A2) and, with an appropriate field index m, to control the equilibrium position of the plasma for the entire range of plasma conditions encountered during a pulse (with I increasing from zero to its maximum value, β_θ from zero to approximately unity, while the internal inductance parameter l_i can vary between 0·1 for a skin current to about 3 for a centrally peaked distribution). Thus, for the conditions of LT-4, the control coefficient Γ (equation A2) must be varied typically between 2·3 and 3·4. The positions of those windings available for control are shown in Fig. 2. The limited space available for their location results in some compromises, so that an 'ideal' field shape cannot be achieved, the index m varying between 0·6 and 0·7 for the best possible arrangement.

To maintain the correct value of the control field at all times, it is necessary to provide both a current proportional to I, corresponding to $\Delta\Gamma$ constant, and one which accommodates a variation $\Delta\Gamma = \pm 0{\cdot}55$. This first condition is achieved to a good approximation by connecting several control turns, shunted by an appropriate impedance, in series with the primary windings. The variation is obtained by a separate current supply to a second set of control windings, the current being controlled by a negative feedback loop: the major-radius (horizontal) position of the plasma is measured (usually electromagnetically although other sensing signals may be used), and a signal proportional to both the displacement ΔR from the desired position and the current I is used to change the control current so as to minimize $I\Delta R$. In practice, for optimal control, it is necessary also to include signals proportional to $\mathrm{d}(I\Delta R)/\mathrm{d}t$ and $\int I\Delta R\,\mathrm{d}t$. The system used is shown schematically in Fig. 5: the output stage of the push–pull feedback amplifier consists of a series of switched transistors, and provides currents up to ± 800 A in 10 A steps in a current forcing mode. The overall response time of the system is limited by the penetration time of magnetic fields through the vacuum vessel, which has been measured to be about 100 μs for vertical fields. The closed loop response is optimized by experimentally adjusting the ratio of the input control signals. A technical description of the feedback arrangement will be presented elsewhere.

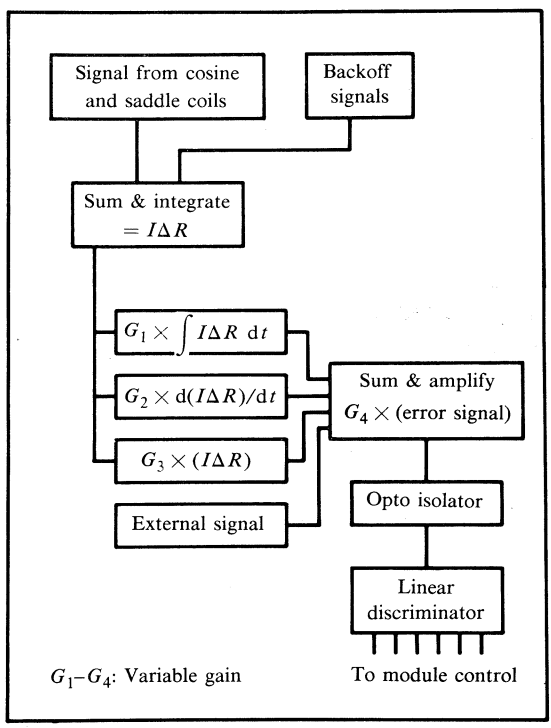

Fig. 5. Schematic representation of the position feedback control system.

Due to the imperfect field geometry, the plasma column is at best only marginally stable to axial (vertical) motion, so that very small asymmetries lead to rapid vertical displacement of plasma and its subsequent loss to the walls. It is therefore necessary also to control the vertical position by providing an appropriate transverse (horizontal) field component B_R to produce a restoring force: this is achieved using a second

feedback arrangement driving a further set of control windings, the control signals being this time proportional to the current times the vertical displacement, $I\Delta z$, from the median plane, and its derivative and integral. The circuit design used is essentially the same as that for the horizontal position control, but with half the current output capability, i.e. ± 400 A in 10 A steps. Both horizontal and vertical feedback amplifiers derive their current from a very low impedance supply based on lead–acid batteries shunted by low internal impedance capacitors.

During the current pulse itself, the effects of any stray fields are automatically compensated by the feedback system. However, as stated above, since it is important that the fields are also corrected at the time of initial breakdown, two further sets of windings are reserved for B_R and B_z correction, each supplied by its own separate motor generator.

The overall level of performance of the position control system is very high; plasma position control to better than 1 mm in both R and z is regularly achieved during routine operation (see Section 4). The feedback system has been used to hold the plasma at positions up to 3 cm off the machine minor axis, involving shifts in either or both of z and R. Maintenance of position in these circumstances is only marginally inferior to that for on-axis operation.

3. Principal Diagnostics

Diagnostic access to the plasma is via the rectangular and circular ports referred to in Section 2*a* and by signals derived from electromagnetic flux changes in various loops external to the plasma. A good description of modern diagnostics for tokamaks has been given by the TFR group (Equipe TFR 1978).

The following subsections describe the main diagnostics in routine use.

(*a*) *Electromagnetic Induction*

This consists of

(1) Loop voltage V: obtained directly from poloidal flux changes in four loops encircling the torus azimuthally, located at $R = 39$, 61 cm, and $z = \pm 11$ cm.

(2) Plasma current I: obtained from an electronically integrated signal from a Rogowski coil outside the shell.

(3) Position of plasma current: derived from the distribution of the poloidal field B_θ measured outside the torus using sine–cosine coils.

(4) Various arrays of small pickup coils (Mirnov coils), arranged to measure the azimuthal and poloidal variations in the local magnetic field due to the plasma, are used to measure and identify (by correlation analysis) the mode numbers of MHD disturbances.

(*b*) *Electromagnetic Emission*

Those parts of the electromagnetic emission spectrum of interest include the line radiation from impurities and neutral hydrogen in the visible and ultraviolet regions; continuum radiation (due to bremsstrahlung and radiative recombination) as soft X-rays (1–10 keV); magnetic bremsstrahlung (incoherent cyclotron harmonic emission) from the plasma electrons, as well as partly coherent radiation due to collective effects in the region $100\,\mu\text{m} < \lambda < 5$ mm; and hard X-rays (from 100 keV to a few MeV) generated from runaway electrons impinging on solid objects, e.g. the limiter. The various regions are monitored as follows:

(i) The region 200–700 nm is monitored by conventional monochromator/photomultiplier apparatus, to follow the time history of various impurity ion species for example. The incompletely ionized states of light atoms (O, N, C) are restricted to the colder ($T_e < 50$ eV) outer regions of the plasma. The H_α line emission is also monitored: its absolute intensity can be related fairly readily to the local ionization rate (Johnson and Hinnov 1973), and its spectral profile (by means of a six-channel high resolution polychromator) is used to derive the temperature of the ions, which are closely coupled by charge exchange to the residual neutral hydrogen atoms.

(ii) The soft X-ray continuum is studied by two methods:

(A) The photon spectrum in the range 1–40 keV is measured by pulse height analysis using a cooled ultra-pure silicon detector. In practice, due to counting limitations, averaging over several shots is necessary. The spectral distribution obtained is characteristic of the peak electron temperature $T_e(0)$ (plasma core), while the absolute intensity is a sensitive measure of the impurity ion content and can be related to the effective charge number

$$Z_{\text{eff}} = \sum_i n_i Z_i^2 \Big/ \sum_i n_i Z_i,$$

where n_i is the number density of ions with charge Z_i (von Goeler *et al.* 1975).

(B) The time- and space-resolved total soft X-ray emission (1–12 keV) is recorded by an array of silicon surface barrier detectors. Since the recorded signal varies with local plasma parameters as $n_e^2 T_e^\alpha$, where $\alpha = 2$–3 depending on the particular filter and detector used, this is a convenient way of identifying and studying regions inside the plasma where local MHD activity occurs, since this usually results in strong variations in local temperature and density. Such localized activity can be used to identify the position corresponding to the $q = 1$ rational surfaces. Furthermore, a convenient measure of electron temperature can be obtained by using detectors in pairs, behind different absorbing filters. The temperature is directly related to the ratio of the signals. The time resolution of these measurements is typically ~ 10 μs.

(iii) The emission in the far-infrared (100 μm – 5 mm) region is continuously monitored using InSb detectors cooled to 4 K. This emission is dominated by radiation at the second harmonic of the electron cyclotron frequency $2\omega_{ce}$ (Celata and Boyd 1977). The magnetic field across the torus varies as $1/R$ so there is a one-to-one correspondence between major radius and emission frequency. Under typical conditions and with a thermal (Maxwellian) plasma the emission at $2\omega_{ce}$ is at the blackbody level corresponding to the local electron temperature, so that the temperature profile can be derived from the $2\omega_{ce}$ spectrum. If runaway electrons are present, enhanced radiation occurs at all cyclotron harmonics, with an observable relativistic frequency shift.

Three methods are used to measure the electron cyclotron emission (ECE). Firstly, the total radiation is routinely monitored for every shot. This shows the global temperature evolution, and also indicates if runaways are present. Secondly, a complete spectrum is measured every 10 ms with a mechanically scanned grid-polarization interferometer (Martin 1982; How and Whitbourn 1983). Fig. 6*a* shows the spectrum of a well thermalized (i.e. Maxwellian) plasma, and the derived temperature profile, while Fig. 6*b* shows a spectrum, taken towards the end of the shot, with a high concentration of runaway electrons. Thirdly, fixed frequency emission can be

studied as a function of time using Fabry–Perot interferometers, which use grids as the reflecting elements. These are useful for observing simultaneously the centre and the edge temperatures as a function of time.

(iv) Hard X-rays (>100 keV) are emitted when 'runaway' electrons (i.e. those accelerated freely by the applied electric field) collide with a solid target, usually the limiter. These are monitored by NaI scintillator/photomultiplier detectors outside the torus. In addition, specially designed probes can be inserted into the outer regions of the plasma (as defined by the limiter) to detect runaway electrons impinging on their small (2 mm wide) tip (Cheetham *et al.* 1983).

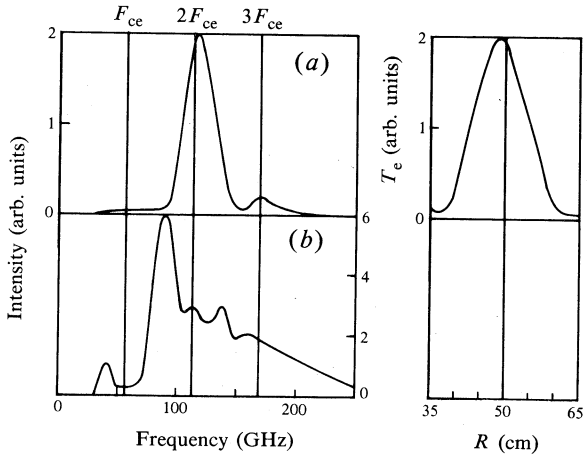

Fig. 6. Two examples of ECE spectra: (*a*) shows a typical spectrum of a thermal discharge and the derived temperature profile; (*b*) shows a spectrum, taken later in the shot, that is dominated by runaway electron emission.

(*c*) *Interferometry*

The electron density is monitored continuously by measuring the phase shift suffered by a beam of radiation of free-space wavelength $\lambda = 337\ \mu$m, derived from a CW HCN discharge laser (Belland *et al.* 1975, 1976; Whitbourn 1984) which traverses a vertical chord of the plasma.

The double interferometer arrangement used, which is described in detail elsewhere (Veron 1974), is capable of measuring phase shifts as small as $\pi/20$, corresponding to changes in the line integral density $\int n_e\, dl$ of $1{\cdot}7 \times 10^{13}$ cm^{-2}. The whole system is mounted on rails. By horizontally displacing the monitoring beam the measurement can be repeated at different chords, and the line integrated densities so obtained can be Abel inverted to yield the density profile $n_e(r, t)$ throughout the discharge.

(*d*) *Thomson Scattering*

The absolute electron temperature and relative density are obtained at a single position and time during a shot by measuring the spectral distribution of photons scattered non-collectively by the electrons from a beam of radiation from a Q-switched ruby laser ($\lambda = 694{\cdot}3$ nm). The source consists of an oscillator operating in a single mode followed by two amplifier stages, and produces a 'clean' pulse of duration ~20 ns and energy content 2–6 J with beam divergence <1 mrad. The receiver

uses a holographic grating as the dispersion element and a detector array of up to eight photomultipliers each sampling a pre-determined wavelength band, typically 5 nm wide. The charge collected by each photomultiplier is recorded digitally by an ADC (LeCroy Type 2250L), gated open for the duration of the scattered signal, and compared with that collected in the same gate width but 10 μs before the laser is fired, to allow for the plasma emission itself. Since the number of photons received in each wavelength channel is typically ~ 100, extreme care is taken both in optical alignment, and in minimizing both the scattered radiation from the laser beam (which contains $\sim 10^{19}$ photons) reaching the detectors, and any cross-talk between channels.

The entire system is aligned and calibrated *in situ* using both Rayleigh scattering from N_2 and a standard lamp. Since the Bragg scattering length defined by the wavelength and angle is much less than the Debye distance in the plasma, the scattered photons are uncorrelated, the spectral distribution being determined only by the uncorrelated thermal motions of the scattering electrons. Thus the scattered spectrum is approximately gaussian with a half-width $\Delta\lambda_{1/2}$ which may be directly related to the electron temperature by

$$T_e = 1 \cdot 32 \times 10^{-3} \{\Delta\lambda_{1/2}/\sin(\tfrac{1}{2}\theta)\}^2 \text{ eV},$$

where λ is in Å and θ is the scattering angle (see e.g. Evans and Katzenstein 1969). The measurement is localized to a plasma volume (determined by the beam divergence and receiver entrance aperture) approximately 1 cm vertically by 1 mm horizontally. The entire laser and receiver system is rigidly mounted on a single structure. This can be moved both vertically and horizontally without affecting the optical alignment, so that localized measurements of electron temperature and density can be made over most of the plasma cross section.

We note that, since time-dependent profiles can be obtained only from many successive shots, this measurement (which is the only completely unambiguous and absolute one available) is used in conjunction with those outlined above which provide continuous monitoring of the plasma properties.

(*e*) *Data Acquisition and Analysis*

It is characteristic of this type of experiment that large amounts of data are obtained during the event (i.e. within 200 ms) with relatively long intervals (typically 4–5 min) between shots. To accommodate this feature, all data acquired during a pulse, at sampling rates which are set between 5 kHz and 2 MHz, are placed into buffer store and transferred to the computer memory during the interval between shots for subsequent treatment. The LT-4 system uses up to 70 channels of CAMAC controlled ADCs in conjunction with a network of small PDP/11 computers to handle about 200 kbytes of data per shot. The network (Vance 1982; Corbould and How 1984) consists of a host plus several satellites (Fig. 7). One satellite handles all CAMAC crates, with the others, each with its own processor, 60 kbyte memory and graphics terminal, being used for analysis. The data is transferred to the disc within 30 s, after which it is accessible to any satellite for processing; for example, for routine graph plotting, correlation and Fourier analysis, temperature derivations etc. The system is very flexible and can readily be extended to accommodate new diagnostics by adding further satellites (up to 14). The arrangement allows all data programs and peripherals to be shared. In addition, the laboratory system is directly linked to a central VAX 11/780 computer supporting more sophisticated analysis programs.

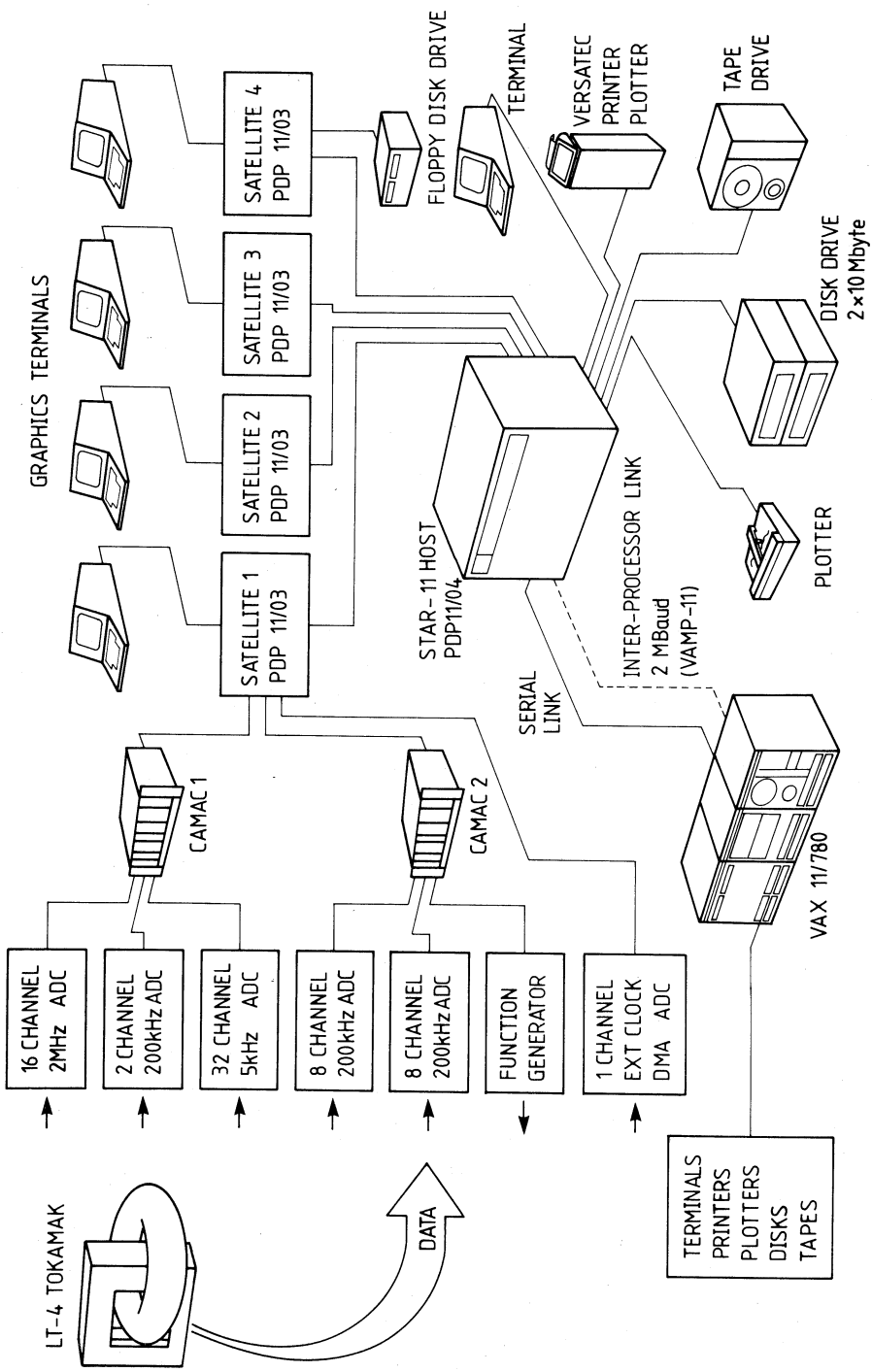

Fig. 7. Schematic representation of the LT-4 data acquisition and analysis system.

4. Typical Operation

In practice, operating conditions such as plasma electron density, current and toroidal magnetic field strength are chosen according to the type of plasma phenomena being investigated (e.g. stable or unstable behaviour), while the pre-set equilibrium control fields are adjusted so that the feedback controlled contribution is minimized.

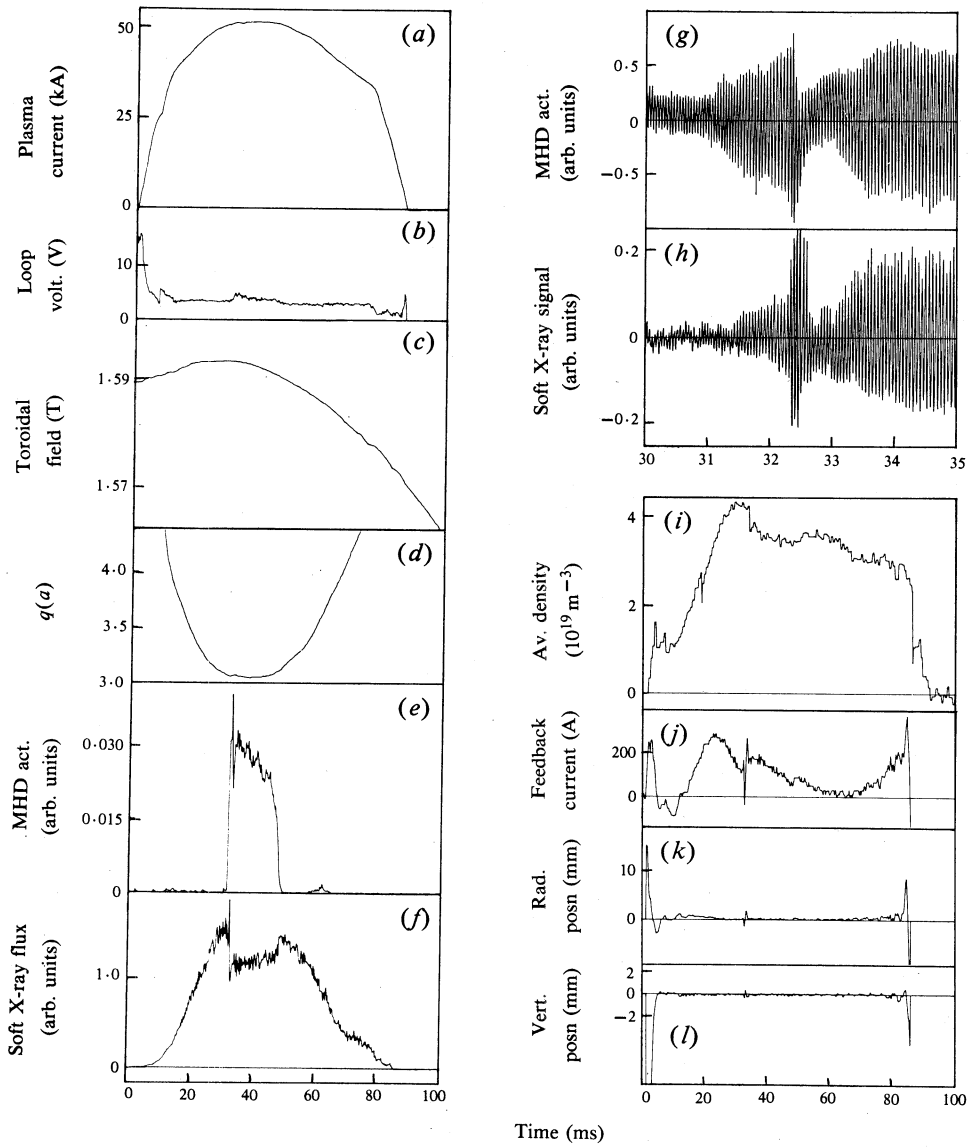

Fig. 8. Data from a typical shot exhibiting strong MHD activity: (*a*) plasma current (kA); (*b*) loop voltage (V); (*c*) toroidal field (T); (*d*) safety factor $q(a)$; (*e*) amplitude of MHD activity; (*f*) soft X-ray flux at $r = 0$; (*g*) MHD activity (expanded); (*h*) soft X-ray signal; (*i*) average electron density (10^{19} m^{-3}); (*j*) radial feedback current (A); (*k*) radial position (mm); (*l*) vertical position (mm).

To a large degree, the plasma confinement and general behaviour is determined by the location of various 'mode-rational' surfaces for which the value of q (see the Appendix) is a small integer. This arises because helical perturbations which vary as $\exp\{-i(m\theta - n\phi)\}$ are resonant on such surfaces if $q = m/n$. For a given current distribution $j(r)$, $q(r)$ can be related directly to

$$q(a) = 2\pi a^2 B/\mu_0 RI,$$

the value at the periphery.

To illustrate some of the typical behaviour as well as the significance of the quantity $q(a)$, we present some traces extracted from the time-dependent data recorded from two discharges (made during a recent investigation of the MHD stability properties), whose main parameters differ only in the strength of the stabilizing toroidal field, with the current (53 kA), electron density and geometry being the same in each case. The first case, for which $B_T = 1{\cdot}6$ T, so that $q(a) \sim 3{\cdot}0$, is illustrated in Figs 8 and 9.

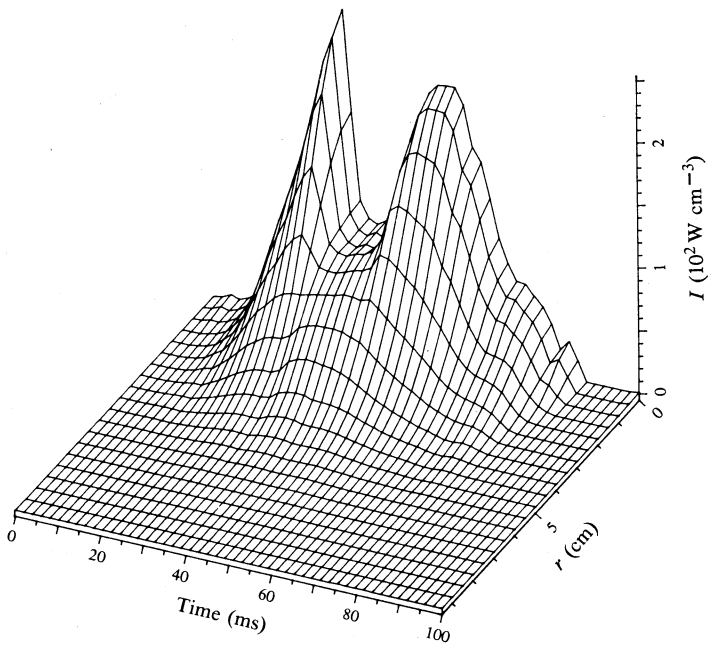

Fig. 9. Temporal evolution of the soft X-ray flux profile for the shot shown in Fig. 8*f*, illustrating strong flattening of the profile due to MHD activity.

The current and toroidal field, shown in Figs 8*a* and 8*c* respectively, vary throughout the pulse (deliberately terminated at $t = 80$ ms), so that $q(a)$ itself varies, as plotted in Fig. 8*d*. The trace in Fig. 8*e* records the amplitude of the poloidal magnetic field fluctuations (Mirnov oscillations) at the torus boundary: it shows a strong burst occurring between 32 and 50 ms, when $q(a)$ is close to $3{\cdot}0$. This burst, shown directly and in an expanded time scale in Fig. 8*g*, can be identified by harmonic analysis as arising from perturbations with mode numbers $m = 1, 2, 3$ and $n = 1$. Soft X-ray emission signals are typified by that shown in Fig. 8*h*. When Mirnov oscillations

are present at their typical frequency of ~20 kHz, they are generally accompanied by oscillations, at the same frequency, in the soft X-ray signals.

The oscillatory nature of the observed activities (typically ~20 kHz) is generally attributed to a rigid rotation of the plasma in the toroidal direction (Equipe TFR 1982): this aspect is currently being investigated.

Some of the macroscopic effects due to the fluctuations can be illustrated: for example, Fig. 8*f* shows that the mean X-ray emission decreases sharply during the burst, apparently due to enhanced radial heat transport caused by the turbulence. The global effect can be seen more clearly in Fig. 9. This shows (by Abel inversion of soft X-ray signals from several chords) the variation of the spatial distribution of soft X-ray emissivity throughout the pulse: as well as the centre of the plasma cooling, the temperature profile becomes flatter during the burst.

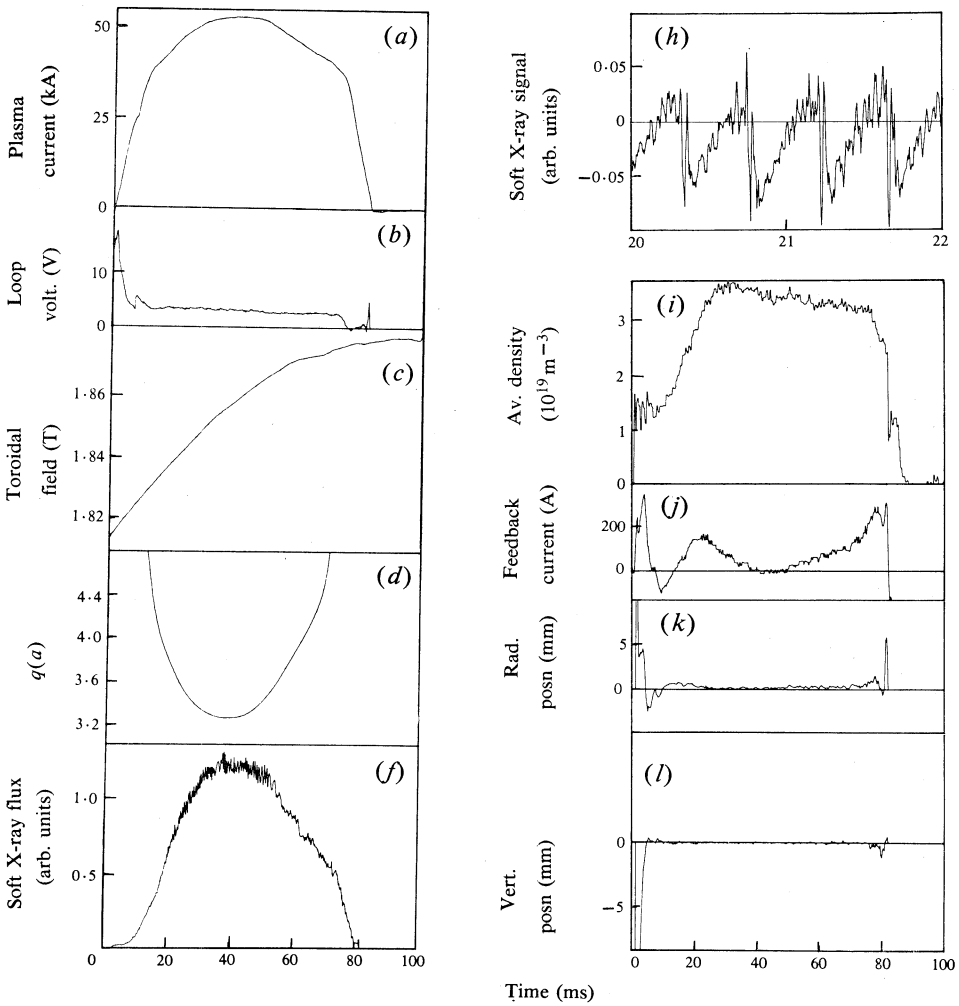

Fig. 10. Data from a shot taken in a regime of no external MHD activity. The labelling is the same as that given in Fig. 8.

Small changes can also be seen in the loop voltage (Fig. 8*b*), caused by the increased plasma resistance, and in the mean density (Fig. 8*i*), caused by slightly enhanced particle diffusion.

More significantly, the sudden redistribution of current and loss of plasma energy (and thus in $\beta_\theta + \frac{1}{2}l_i$) cause a correspondingly abrupt change in the transverse control field required for positional stability. In our case, as shown by the traces in Figs 8*j*, 8*k* and 8*l*, the feedback control system responds sufficiently fast and accurately so that the major radius remains within about 2 mm of its nominal position even during such events.

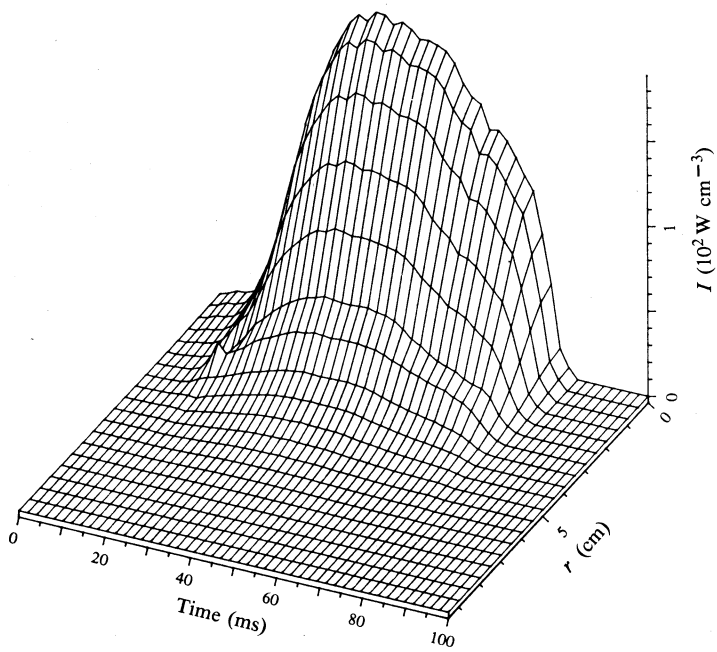

Fig. 11. Temporal evolution of the soft X-ray flux profile for the shot shown in Fig. 10*f*.

The effect of increasing the stabilizing magnetic field to about 1·8 T is shown in Figs 10 and 11, where we have retained the same labelling for ease of comparison. In this case $q(a)$ remains above 3·3. The level of external fluctuation is now very small, being barely observable above instrumental noise, but the internal sawtooth activity is clearly seen on the central X-ray signal. The sudden changes in observables no longer occur, so that all quantities vary smoothly, as shown in the traces in Figs 10*f* and 10*i*, which may be directly compared with those in the earlier examples. The X-ray temperature profile remains smooth throughout the discharge, while the plasma is held to well within 1 mm of its nominal position for the feedback system.

During normal operation, up to more than 70 channels of data are acquired, at various sampling rates up to 2 MHz. The samples shown above are intended merely to illustrate some of the phenomena observed. Fuller details of particular observations will appear in subsequent papers.

5. Concluding Remarks

The LT-4 tokamak described here includes several notable technical features, such as good flexibility and unusually uniform toroidal field, in spite of the close proximity of the conductors to the plasma and the high currents employed. It is also historically unique in being the first fusion device to be powered by a homopolar generator.

From the experimental viewpoint its performance is characterized by a high degree of reproducibility, which we believe results from the combination of a short time-constant vacuum shell and a very responsive feedback system which allow exceptionally precise positional control to be maintained even while traumatic changes occur inside the plasma. This makes LT-4 particularly well suited to studies of such traumatic activity, including the disruptive instability, since it allows transient plasma phenomena to be studied without being complicated by plasma–wall interactions.

Acknowledgments

The construction and operation of this complex apparatus has involved many technical and workshop staff, to whom we are most grateful. Special thanks are due to R. Goldberg, G. C. J. Davies, R. J. Kimlin, G. L. Ostheller, M. A. Corbould, G. McCluskey and the Homopolar Generator team.

We also acknowledge financial assistance from the Australian Atomic Energy Commission, the Australian Institute for Nuclear Science and Engineering and the National Energy Research, Development and Demonstration Program of the Department of National Development and Energy.

References

Artsimovich, L. A. (1972). *Nucl. Fusion* **12**, 215–52.
Bateman, G. (1978). 'MHD Instabilities' (M.I.T. Press).
Belland, P., Vernon, D., and Whitbourn, L. B. (1975). *J. Phys.* D **8**, 2113.
Belland, P., Vernon, D., and Whitbourn, L. B. (1976). *Appl. Opt.* **15**, 3047.
Bickerton, R. J. (1977). Review of tokamak experiments. UKAEA Rep. No. CLM-R176.
Blamey, J. W. (1978). 'High Power High Energy Pulse Production and Application' (Ed. I. K. Inall), p. 14 (Aust. Nat. Univ. Press).
Celata, C. M., and Boyd, D. A. (1977). *Nucl. Fusion* **17**, 735.
Cheetham, A. D., How, J. A., Hogg, G. R., Kuwahara, H., and Morton, A. H. (1983). *Nucl. Fusion* **23**, 1694.
Corbould, M. A., and How, J. A. (1984). A network approach to large-scale experimental data acquisition and analysis. *Comput. Phys. Commun.* (in press).
Equipe TFR (1978). *Nucl. Fusion* **18**, 647.
Equipe TFR (1982). Minor and major disruptions in the TFR tokamak. EURATOM Rep. No. EUR-CEA-FC-1151.
Evans, D. E., and Katzenstein, F. (1969). *Rep. Prog. Phys.* **32**, 207.
Furth, H. P. (1975). *Nucl. Fusion* **15**, 487–534.
Hollis, M. J. (1978). Proc. Conf. on Electrical Energy, p. 183 (Institution of Engineers: Sydney).
How, J. A., and Whitbourn, L. B. (1983). *Int. J. Infrared Millimeter Waves* **4**, 335.
Johnson, L. C., and Hinnov, E. (1973). *J. Quant. Spectrosc. Radiat. Transfer* **13**, 333.
Martin, D. H. (1982). *In* 'Infrared and Millimeter Waves' (Ed. K. J. Button), Vol. II, Ch. 2 (Academic: New York).
Morton, A. H. (1981). *Aust. Physicist* **18**, 195.
Mukhovatov, U. S., and Shafranov, V. D. (1971). *Nucl. Fusion* **11**, 605.
Rebut, P. H. (1984). Proc. 11th European Conf. on Controlled Fusion and Plasma Physics, Aachen (Ed. S. Methfessel) (European Physical Society) (to be published).

Sheffield, J. (1981). *Proc. IEEE* **69**, 885–917.
Vance, C. F. (1982). Proc. 9th Australian Computer Conf. (Eds A. H. J. Sale and G. Hawthorne), p. 871 (Aust. Computer Soc.).
Veron, D. (1974). *Opt. Commun.* **10**, 95.
von Goeler, S., Stodiek, W., Eubank, H., Fishman, H., Grebenshchikov, S., and Hinnov, E. (1975). *Nucl. Fusion* **15**, 301.
Weldon, W. F., Rylander, H. G., and Woodson, H. H. (1978). *In* 'High Power High Energy Pulse Production and Application' (Ed. I. K. Inall), p. 281 (Aust. Nat. Univ. Press).
Whitbourn, L. B. (1984). *Int. J. Infrared Millimeter Waves* **5**, No. 5.
Young, K. (1984). Proc. 11th European Conf. on Controlled Fusion and Plasma Physics, Aachen (Ed. S. Methfessel) (European Physical Society) (to be published).

Appendix. The Tokamak Configuration

The quasi-cylindrical coordinates used here are shown in Fig. 12 and the principal features of a tokamak in Fig. 13.

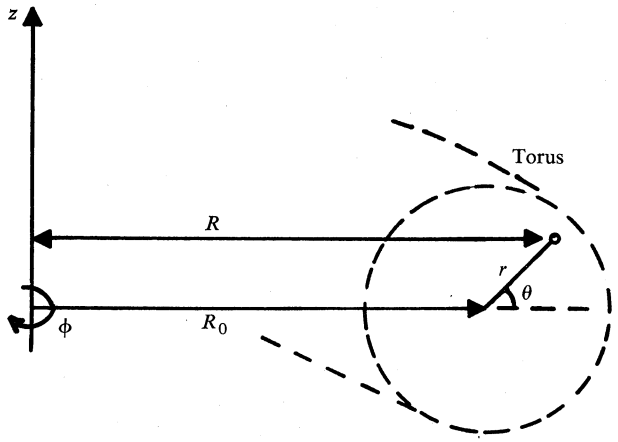

Fig. 12. Representation of the quasi-cylindrical coordinates (r, θ, ϕ).

In order for a hot toroidal plasma column to be maintained in equilibrium in the presence of those forces (resulting for example from the finite plasma kinetic pressure p and electromagnetic forces) which try to expand it in both major and minor radii, it is necessary to provide a suitable combination of toroidal, poloidal and axial fields (designated here by B_ϕ, B_θ, B_z), ordered (in the case of a tokamak) by $B_\phi > B_\theta \sim B_z$ such that the resultant fields form closed, nested magnetic flux surfaces (defined by $\boldsymbol{B}.\nabla\boldsymbol{B} = 0$). In the case of a tokamak, the poloidal field B_θ is that due to a ϕ-directed current in the plasma itself. Such equilibria can be obtained by numerical solution of the ideal MHD equation for force balance

$$\boldsymbol{j} \times \boldsymbol{B} = \nabla p, \tag{A1}$$

with boundary conditions etc. chosen to correspond to typical operation of the LT-4. In equation (A1) the current density $\boldsymbol{j}$ and magnetic field $\boldsymbol{B}$ include the contributions of self-consistent currents in the plasma and their associated fields.

We note that for such an equilibrium to be sustained, the distributions of both the plasma current

$$I = 2\pi \int_0^a r j(r)\, \mathrm{d}r$$

and plasma pressure

$$p(r) = \sum_s n_s(r)\, T_s(r),$$

where n_s and T_s are respectively the number and density temperature of charged particles of species s, must be maintained constant. In practice, a quasi-steady state is achieved by maintaining both the total current and particle density constant (from external sources), thus simultaneously balancing the ohmic heating against the radial heat loss, and the rate of ionization against charged particle loss. It is interesting to note that it is only in recent years that experimental techniques have improved sufficiently to maintain such steady-state conditions (taken as those with durations much longer than all characteristic loss times): equilibria lasting several seconds can now be achieved in larger machines, the longest being limited by technological factors rather than by plasma processes.

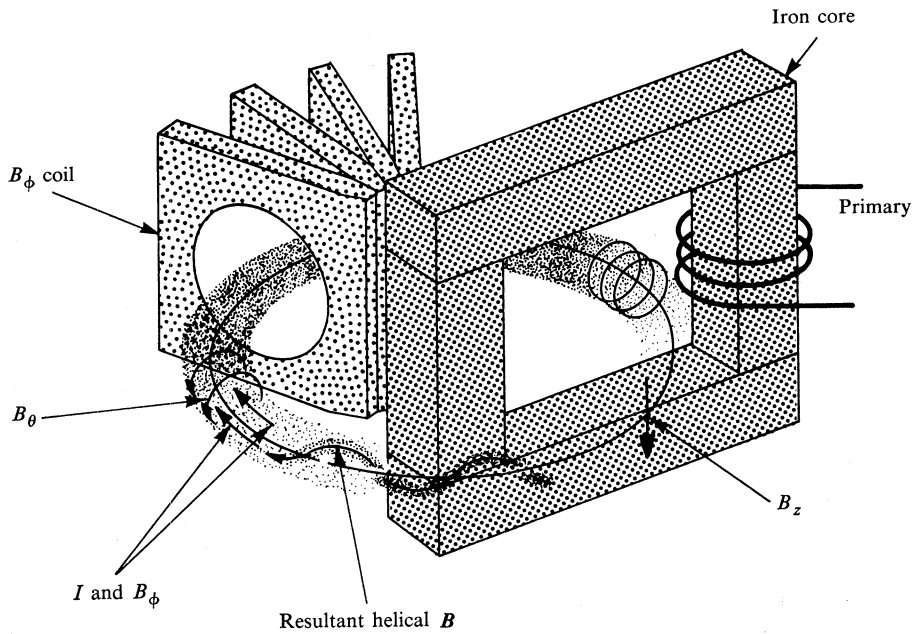

Fig. 13. Tokamak geometry.

In general the plasma pressure decreases monotonically with increasing minor radius, the isobars coinciding with the magnetic surfaces. The outermost useful surface at $r = a$ is in practice usually defined by a physical obstacle known as the limiter, beyond which j and p are approximately zero. For sufficiently low plasma pressure [$\beta = p/(B^2/2\mu_0) \ll 1$] the surfaces are usually approximately circular in cross section, with the magnetic axis displaced to a larger major radius than that of the limiting surface. As β increases, the surfaces become distorted and the displacement of the axis becomes larger (Mukhovatov and Shafranov 1971).

The magnetic fields are provided by currents in several sets of windings together with the plasma current itself (see Fig. 13). The main toroidal field B_ϕ is produced by solenoidal currents in θ-directed windings; the poloidal field B_θ is due to the ϕ-directed plasma current induced through flux changes in the transformer core (which may be iron or air) while the remaining, mainly axial, 'control' field components are produced by externally drawn currents in ϕ-directed conductors encircling the plasma axis and outside the plasma itself. We note that, with the exception of the limiter which is usually localized in ϕ, the whole system is axisymmetric.

Such equilibria require that the strength of the control field, and to a lesser extent its spatial variation, is very precisely determined. The transverse (axial) field required on the minor axis is given by (Mukhovatov and Shafranov 1971)

$$B_z = (\mu_0 I/4\pi R)(\ln 8Ra^{-1} - \tfrac{3}{2} + \tfrac{1}{2}l_i + \beta_\theta) \equiv (\mu_0 I/4\pi R)\Gamma, \tag{A2}$$

where $\mu_0 l_i/4\pi$ is the internal inductance per unit length of the plasma column and

$$\beta_\theta = 8\pi^2 a^2 \langle p \rangle / \mu_0 I^2$$

is the ratio of plasma pressure to that exerted by the poloidal field at the boundary. To ensure axial stability, the field index

$$m = (R/B_z)(\partial B_z/\partial R)$$

should (for circular cross-section outer magnetic surfaces) lie in the range $0 < m < 0{\cdot}6$. Since both l_i and β_θ depend on detailed plasma conditions they will, in practice, vary considerably during a given discharge.

Since the plasma has very low inertia, any small unbalanced force can result in very rapid motion unless restrained magnetically, for example, by eddy currents induced in the torus wall. When, as in modern tokamaks such as LT-4, these currents decay quickly, it is necessary to rapidly adjust the control fields correspondingly, for example, by feedback control, in order to compensate both for rapid changes in plasma conditions as well as for unavoidable stray magnetic fields and asymmetries arising from, for example, electrical connections or core flux leakage.

An important geometrical parameter, which determines the plasma stability to helical modes, is the number q which describes the helicity of the field lines which trace out the various magnetic surfaces; for a circular cross section this has the simple form

$$q(r) = rB_\phi/RB_\theta. \tag{A3}$$

For the radial current distributions usually encountered in tokamaks $\partial j/\partial r < 0$, so that $q(0) < q(a)$. In general, MHD stability requires $q(a) > 2$–3, while $q(0) > 1$. The value at the edge of the plasma $q(a)$ is related to the total current (for circular cross sections) by

$$q(a) = (2\pi/\mu_0)(a^2\beta_\phi/R_0 I). \tag{A4}$$

Surfaces for which $q = m/n$, where m and n are small integers, are known as rational surfaces and have special properties.

For $q < 2$ and for non-circular cross sections and small aspect ratios R/a, these geometrical definitions of q should strictly be replaced by ones defined from flux coordinates (Bateman 1978).

Manuscript received 25 November 1983, accepted 17 January 1984